Journal of Applied Polymer Science

WILEY

Applied Polymer SCIENCE

RESEARCH ARTICLE OPEN ACCESS

Effect of Few-Layer Graphene (FLG) and Relative Photodegradation Depth on the Ductile to Fragile Transition of High-Density Polyethylene

Samira Karimi[1] | Emna Helal[1,2] | Gabriel Matheus Pinto[1] | Giovanna Gutierrez[2] | Nima Moghimian[2] | Tatiana Parra Vello[3,4] | Guilhermino José Macêdo Fechine[3,4] | Eric David[1] | Nicole Demarquette[1]

[1]Mechanical Engineering Department, École de Technologie Supérieure, Montréal, Canada | [2]NanoXplore Inc., Quebec, Canada | [3]Engineering School, Mackenzie Presbyterian University, São Paulo, São Paulo, Brazil | [4]Mackenzie Institute of Research in Graphene and Nanotechnologies—MackGraphe, Mackenzie Presbyterian Institute, São Paulo, São Paulo, Brazil

Correspondence: Guilhermino José Macêdo Fechine (guilherminojmf@mackenzie.br) | Nicole Demarquette (nicoler.demarquette@etsmtl.ca)

Received: 28 August 2025 | **Revised:** 6 November 2025 | **Accepted:** 6 November 2025

Funding: This work was supported by the Natural Sciences and Engineering Research Council of Canada (NSERC) (Grant CRDPJ 538482-18), and the Canadian Research Chairs (CRC Tier 1-2021-00489).

Keywords: aging | crystallization | degradation | fullerenes | graphene | mechanical properties | nanotubes

ABSTRACT

Photo-stabilization is essential for thermoplastics in outdoor applications, as it extends service life by protecting polymer chains from UV-induced degradation. Graphene has emerged as a multifunctional stabilizer with capabilities including UV screening, barrier effects, and radical scavenging. However, its influence on the depth profile of photodegradation under UV exposure is not fully understood. This work investigates the effect of few-layer graphene (FLG) on the photodegradation of high-density polyethylene (HDPE). Neat HDPE and composites with 0.5 wt% FLG were prepared in two thicknesses (3 and 2 mm) and exposed to UV radiation for varying durations. Elongation at break was measured as a function of exposure time and correlated to the degradation depth, determined by chemi-crystallization using Raman microscopy. In neat HDPE, embrittlement occurred when the degraded layer reached ~10% of the thickness, after 10 and 7 days for 3- and 2-mm samples, respectively, preceding the appearance of surface cracks. In contrast, HDPE with 0.5 wt% FLG retained 50% of its initial elongation at break, characterizing a ductile failure, even after 45 days despite surface cracks. Additionally, embrittlement was only observed when the relative degradation depth reached 12.5%, exceeding the 10% threshold observed for the neat HDPE. The persistence of ductility is attributed to the photo-stabilizing effect of FLG and the detachment of the degraded surface from the ductile core, leading to a material with enhanced UV resistance for outdoor packaging and coating applications.

1 | Introduction

Research on the photo-stabilization of polymers has been ongoing for several decades, with a particular focus on understanding the mechanisms of photodegradation and developing methods for photo-stabilization [1–5]. Photo-stabilization is essential for polymers used in outdoor applications, such as in construction, recreation, protective paints, and coatings. Among the potential stabilizers, graphene derivatives have emerged as a promising candidate for specific polymer applications, as it has been shown by several works that it can act on multiple fronts, that is, screening/absorbing the UV radiation, suppressing the diffusion of oxygen in the material, and also scavenging potential radicals formed [6–14]. However, the effectiveness of graphene as a stabilizer can depend on several critical factors, including the content employed, UV exposure duration, and

part thickness. All these factors play a crucial role in the extent of degradation in any given application.

Concomitantly, it has been demonstrated that photodegradation of polymers is associated with structural changes at the molecular level, which vary along the thickness of a sample exposed to UV radiation [15]. In semi-crystalline polymers such as HDPE, chemical alterations during degradation lead to chain scission and consequently, to chemi-crystallization [16], reduced interlamellar spacing, decreased tie molecule concentration, and ultimately, embrittlement [17–21]. This results in a transition from ductile to brittle behavior in the material, which is inherently linked to the ratio between the photodegradation depth and the material's thickness. This ratio is further referred to as relative photodegradation depth.

It has been demonstrated that the photodegradation depth of a stabilized polymer depends on the efficiency and UV stabilizing mechanism of the photo-stabilizer. In particular, in the case of UV reflectors and screeners, photodegradation can be confined to the region near the exposed surface [22]. Therefore, in order to understand the effectiveness of UV stabilizers, it becomes imperative to evaluate the photodegradation depth and the microstructural changes beneath the polymer's UV-exposed surface.

The photodegradation depth in polymers is defined by the depth of the material that undergoes chemical and microstructural changes due to the UV exposure. It has been studied using various techniques, including DSC (differential scanning calorimetry) [23], SEC (size exclusion chromatography), and ATR-FTIR (attenuated total reflectance Fourier transform infrared spectroscopy), which involve extracting samples from different depths using a microtome [24]. For example, Gulmine et al. [24] investigated changes in crystallinity and chemi-crystallization during photodegradation of 3 mm thick HDPE and LDPE samples as a function of sample depth. The results showed chemi-crystallization remained confined to a depth of 500 μm after 6 weeks of UV exposure. However, to the best of the authors' knowledge, no investigation has examined the photodegradation depth of a graphene-reinforced polymer composite by correlating microstructural changes in the polymer matrix with the resulting macroscopic properties.

Thus, this work aims to investigate the effect of adding a commercial few-layer graphene (FLG) on the photodegradation depth of HDPE. The samples' photodegradation depth was evaluated and correlated to macroscopic physical properties, specifically the transition from ductile to brittle behavior. To achieve this, neat HDPE and its composite containing 0.5 wt% FLG, with thicknesses of 3 and 2 mm, were exposed to UV radiation under humid conditions. The specific FLG content used in this study was selected based on the findings from our previous work, in which this concentration demonstrated the highest efficiency in protecting the polymer against UV-induced degradation [8]. In that work, a detailed analysis of the photoprotection mechanisms revealed that graphene's contribution to the overall stabilization effect could be attributed to two main pathways. Approximately 57% of the stabilization originated from graphene's ability to absorb/screen harmful UV radiation, thereby preventing photons from reaching and damaging the polymer chains, while the remaining 43% was associated with its radical scavenging capability, effectively neutralizing reactive species generated during photooxidation and slowing chain scission processes [8]. Here, the effective UV dosage corresponding to the exposure time was calculated based on the "Cumulative Damage Model" [25]. The elongation at break and failure zone were tracked based on exposure time and its corresponding UV dosage. Microstructural changes and photodegradation depth were analyzed using Raman spectroscopy coupled with an optical microscope. This approach has the advantage of providing a higher resolution and a nondestructive means of assessing the degradation, that is, all the measurements can be done directly on the cross-section of the part, without the need to extract samples from different depths. Thus, this work aims to unveil the quantitative relationship between photodegradation depth and the resulting embrittlement behavior of the material.

2 | Materials and Methods

2.1 | Materials

In this work, injection grade HDPE (Alathon H5618), purchased from LyondellBasell Co., and FLG (GrapheneBlack 3X), provided by NanoXplore Inc., were used as matrix and photostabilizer, respectively. According to the technical datasheets, this HDPE has a melt flow index (MFI) of 18 g/10 min, a melting temperature of 130°C, and a density of 0.956 g/cm^3. The FLG exhibits a primary particle size of 1–2 μm, agglomerate size with D90 < 70 μm, and a bulk density of 0.2–0.3 g/cm^3. More detailed information can be found in Tables S1 and S2.

2.2 | Composite Preparation

A HAAKE twin-screw extruder, Model Rheomex OS PTW16/40 ($L/D = 40$), was used to prepare HDPE composites containing 0.5 wt% FLG, as well as neat HDPE samples. The process of fabricating HDPE composites involved diluting a 30 wt% HDPE masterbatch to achieve the desired concentration. The processing conditions can be found in a previous work [8], but the screw speed was set to 100 rpm and the temperature profile was 180°C–180°C–180°C–180°C–190°C–200°C–200°C–190°C–190°C–180°C–180°C, from the first heating zone to the die. The feeding rate was set to 7% of the extruder's screw speed, and each sample was extruded twice to obtain a more homogeneous dispersion of FLG within the HDPE matrix.

Three- and two-millimeter thick type V dumbbell-shaped specimens were injection-molded using a microinjection machine (HAAKE MiniJet Pro) under the following conditions: barrel temperature of 160°C, mold temperature of 70°C, injection pressure of 300 bar, injection time of 20 s, holding pressure of 300 bar, and holding time of 15 s.

2.3 | Photodegradation Process and UV Dosage Calculation

The injection-molded samples were subjected to accelerated weathering using a QUV chamber equipped with UVA-340

TABLE 1 | Photodegradation procedure.

Step	Function	Irradiance (W/m^2)	Temperature (°C)	Time (h)
1	UV	0.89	60	8
2	Condensation	N/A	50	4

lamps according to the ASTM D4329 standard. The samples underwent specific exposure conditions described in our previous work [8], that is, 8 h of UV exposure at 60°C, followed by 4 h of water condensation at 50°C. The UV exposure conditions are presented in Table 1. The samples' properties were assessed after being exposed to UV radiation for periods of 4, 7, 10, and 15 days for neat HDPE, while the composites containing 0.5 wt% FLG were assessed for longer exposure times, that is, 30 and 45 days.

Each sample was assigned a label in the format HDPEUV*x*-*z* or HDPE*y*UV*x*-*z*, where x denotes the exposure time in days, y represents FLG concentration, and z indicates the sample thickness. For example, HDPE05UV15-2 corresponds to HDPE containing 0.5 wt% FLG, 15 days of UV exposure, and 2 mm thickness.

In this study, total effective UV dosage, $D_{\text{eff}}\left(\frac{J}{m^2}\right)$, defined by the total effective energy of all the photons received by the sample per unit surface, was estimated based on the "Cumulative Damage Model" described by Equation (1) [25–27]:

$$D_{\text{eff}}(t) = \int_0^t \int_{\lambda_{\min}}^{\lambda_{\max}} E_0(\tau)\Gamma(\lambda)\left(1 - e^{-A(\lambda,\tau)}\right)\emptyset(\lambda)d\lambda d\tau \quad (1)$$

where $\lambda_{\min}$ and $\lambda_{\max}$ denote minimum and maximum effective used UV wavelengths (nm). $A(\lambda, \tau)$ indicates absorbance spectrum of the material at the wavelength of λ. $E_0(\tau)$ denotes UV irradiance (J/s m^2) $\Gamma(\lambda)$ denotes spectral distribution (nm^{-1}), respecting the condition: $\int_0^\infty \Gamma(\lambda)d\lambda = 1$, t = elapsed time (s), and $\emptyset(\lambda)$ is a quasi-quantum yield function that describes the relative damage at the λ wavelength. This function depends on environmental conditions such as temperature and humidity.

In this study, the total effective UV dosage was calculated with the following assumptions:

- Effect of humidity on $\emptyset(\lambda)$ is negligible.
- Thermal degradation is negligible.
- There is no UV radiation transmitted through the sample. Therefore, based on Lambert–Beer's law presented in Equation (2), $A(\lambda, t)$ is infinitely large for the entire duration of the experiment.

$$\ln\left(\frac{I_0(\lambda)}{I(\lambda)}\right) = A(\lambda) \quad (2)$$

where $I_0(\lambda)$ and $I(\lambda)$ are intensities of incident and transmitted light at the λ wavelength.

- The UV source is a monochromatic source, so that $\Gamma(\lambda) = \delta(\lambda - 340)$, where $\delta(\lambda)$ is the Dirac function.

Based on the above assumptions, the total effective dosage can be simplified as:

$$D_{\text{eff}}(t) = \int_0^t E_0(\tau)\emptyset(340)\mathrm{d}\tau \quad (3)$$

For simplicity, and as the QUV spectrum is centered at 340 nm, the UV source is assumed to be monochromatic. The quantum yield for neat HDPE at a wavelength of 340 nm and a temperature around 40°C has been reported to be 8.86×10^{-2} [28, 29]. Considering the fact that quantum yield is an Arrhenius function of temperature [30], and the experimental temperature (60°C) is close to 40°C, and both are above the glass transition temperature of HDPE (−120°C), any significant alteration in quantum yield between 40°C and 60°C was deemed negligible. Consequently, this study employed the quantum yield value of 8.86×10^{-2}. Thus, Equation (3) was employed to calculate the "effective UV dosage" ($D_{\text{eff}}\left(\frac{J}{m^2}\right)$) corresponding to various UV exposure times, as is presented in Table 2. To make a meaningful comparison among samples with different thicknesses, the "effective UV dosage" was normalized to the sample thickness. This normalization allowed the determination of the effective UV dosage per sample volume, also reported in Table 2. In this manuscript, "UV dosage per sample volume" refers to effective UV dosage per sample volume ($\frac{D_{\text{eff}}}{\text{Thickness}}$).

2.4 | Characterizations

The dispersion of FLG across the thickness of the HDPE matrix was analyzed using an Optical Microscope (OM), Carl Zeiss Jena JENAPOL Instrument, on a thin film with a thickness of 50 μm, obtained using a microtome.

A scanning electron microscope, SEM S3600-N Hitachi, with a voltage of 15 kV, was used to observe the surface of the exposed samples. SEM observations were conducted on both the exposed surface and on the side surfaces to analyze the crack density and depth. The samples were coated with a 2 nm layer of gold before being analyzed by SEM. Figure 1 illustrates the exposed and the side surface (cross-section), as well as the crack depth.

The tensile properties of the samples were assessed at room temperature using an MTS Alliance RF/200 testing machine, following the ASTM D638 standard, with a crosshead speed of 50 mm/min. This speed was selected for the tensile tests as the samples fractured within the 5-min interval specified by the standard,

TABLE 2 | Effective UV dosage corresponding to different UV exposure times.

Exposure time (both UV and condensation) (days)	Exposure time (both UV and condensation) (h)	Only UV Exposure time (s)	D_{eff} (J/m²)	$\frac{D_{eff}}{Thickness}$ (J/m³)	
				3 mm thick	2 mm thick
0	0	0	0	0	0
4	96	23.0×10^4	18.2×10^3	60.6×10^5	90.8×10^5
7	168	40.3×10^4	31.8×10^3	10.6×10^6	15.9×10^6
10	240	57.6×10^4	45.4×10^3	15.1×10^6	22.7×10^6
15	360	86.4×10^4	68.1×10^3	22.7×10^6	34.1×10^6
30	720	17.3×10^5	13.6×10^4	45.4×10^6	68.1×10^6
45	1080	25.9×10^5	20.4×10^4	68.1×10^6	10.2×10^7

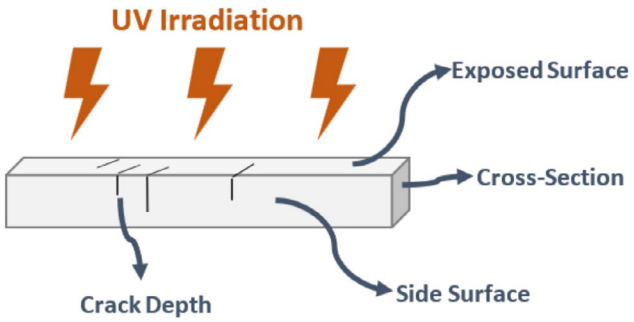

FIGURE 1 | Schematic illustration of the UV-exposed samples. [Color figure can be viewed at wileyonlinelibrary.com]

allowing for observation of the effect of UV exposure on the material's embrittlement and eliminating the need to test additional speeds. Five specimens of each sample were tested. The reported values are the averages obtained from these measurements.

In order to characterize changes in sample microstructure during photodegradation, Raman microscopy was conducted using a Witec alpha 300 system equipped with a 532 nm laser from Witec with a power of 1 mW, and a grating of 1800 g/mm. A 50× objective lens with a numerical aperture of 0.7 was used for imaging. The integration time for each measurement was set to 10 s, and a total of 10 accumulations were performed to enhance the signal-to-noise ratio.

Microstructural changes were investigated by tracking the intensity variation of the Raman band at 1416 cm^{-1}, assigned to the orthorhombic crystalline chains, as a function of UV exposure time and sample depth. To ensure accurate measurements, the intensity of the Raman band at 1416 cm^{-1} was normalized using the CH_2 twisting bands at 1296 cm^{-1} as an internal reference [31, 32], as indicated in Equation (4):

$$\text{Crystal band intensity} = \frac{I_{1416cm-1}(\text{a. u.})}{I_{1296}(\text{a. u.})} \quad (4)$$

where I_{1416} and I_{1298} are the intensities of the Raman bands located at 1416 and 1296 cm^{-1}, respectively.

The corresponding degree of crystallinity was calculated using Equation (5):

$$\text{Crystallinity}(\%) = \frac{\text{Crystal band intensity}}{0.46} \times 100 \quad (5)$$

0.46 is a constant corresponding to the intensity of the peak at 1416 cm^{-1} when HDPE is 100% crystalline [33].

Although other techniques, such as DSC [23], SEC, and ATR-FTIR have already been used to perform such measurements, their conventional operation evaluates the bulk material or a significantly larger region, requiring the extraction of samples from different depths using a microtome [24]. This makes these techniques less practical for such a study and direct comparisons with the Raman measurements less meaningful.

3 | Results

3.1 | FLG Dispersion

Figure 2 presents the HDPE cross-section and dispersion of FLG in HDPE05. It is noticeable that the FLG concentration is lowest in the region close to the surface due to the skin effect during molding, which makes this area especially vulnerable to degradation processes promoted by the UV exposure (Figure 2b). The black arrow indicates the direction from the sample surface toward the bulk, and the red arrows highlight FLG particles.

3.2 | Crack Formation

Figures 3 and 4 show SEM images of the UV-exposed surface and the cross-section of neat HDPE and HDPE05, respectively, for both 2- and 3-mm thick samples, as a function of exposure time. Different scales are used to better illustrate the cracks' dimensions and concentration. The red arrows in Figure 4 indicate the edge of the samples. SEM images of samples before UV exposure are presented in Figure S1.

It can be seen that in the neat 2 mm thick HDPE sample, the first cracks appear after 10 days of UV exposure due to

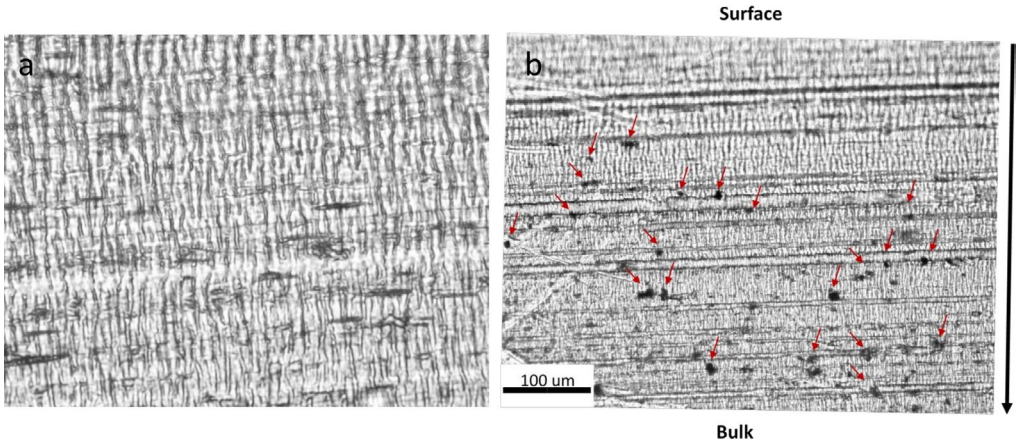

FIGURE 2 | Optical image of (a) HDPE cross-section and (b) FLG dispersion across the cross-section of HDPE05. [Color figure can be viewed at wileyonlinelibrary.com]

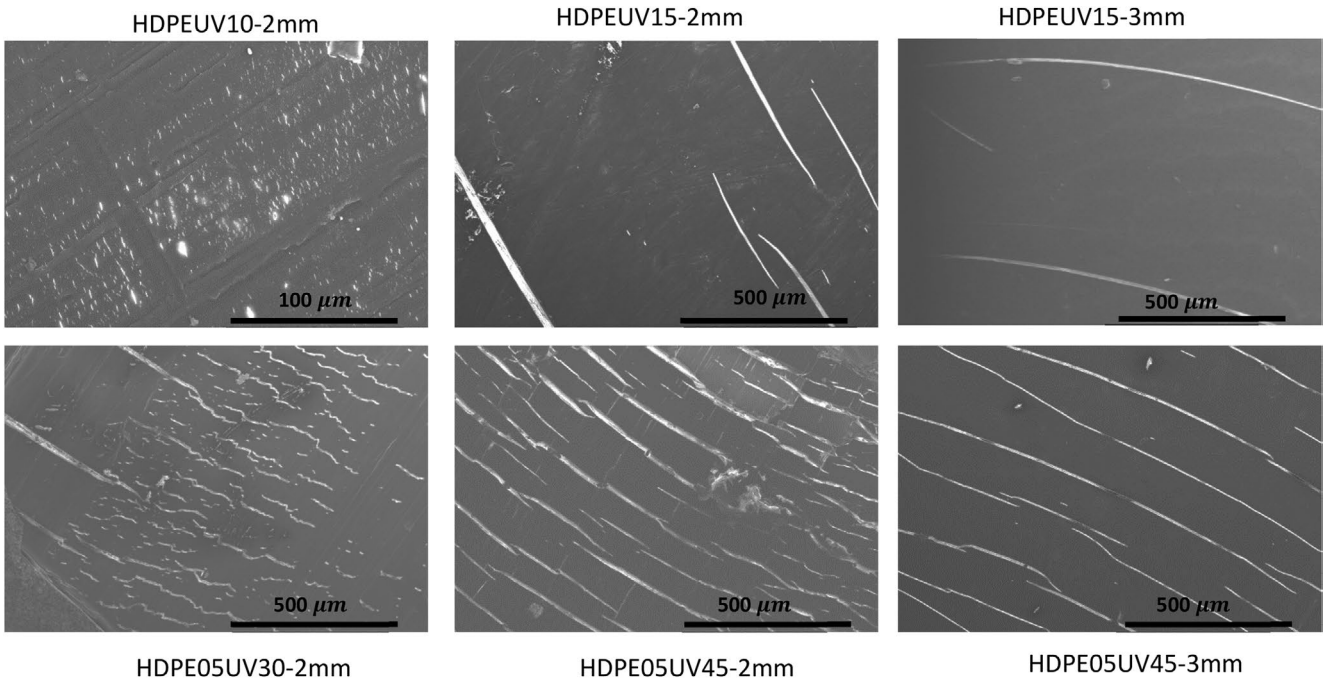

FIGURE 3 | SEM images of the exposed surfaces of neat HDPE and HDPE05 with sample thicknesses of 2 and 3 mm.

chemi-crystallization and stress concentration induced by photodegradation [34].

Conversely, the neat 3 mm thick HDPE sample exhibits higher stability, remaining free from any visible cracks for up to 15 days of UV exposure. Increased stability in the 3 mm thick sample may be attributed to the fact that the relative photodegradation depth is lower than in the 2 mm sample. Moreover, the appearance of cracks on the cross-section provides an indicator of their depth, with the cracks extending throughout the entire thickness in HDPEUV15-2.

In the case of HDPE05, a notable resistance to UV-induced cracks can be observed. The initial cracks, with a depth of 150 μm, become visible only after 30 days of UV exposure in the 2 mm thick sample. As UV exposure time increases to 45 days, both 2 and 3 mm thick HDPE05 samples develop additional cracks with greater depths. The crack depths are reported in Table 3. Furthermore, the size of cracks is significantly smaller in HDPE05 compared to that of neat HDPE, highlighting the stabilizing effect of FLG, not just hindering degradation itself, but also restraining the development of surface cracks.

3.3 | Mechanical Properties

Figure 5 exhibits the stress–strain curves of neat HDPE and HDPE05 specimens for the two thicknesses studied after they were subjected to different exposure times. The curves are divided into four different zones, defined in Table 4, each related to a specific microstructural deformation. The initial segment is labeled as Zone I, or the elastic zone, and it is located before the first yield point. Zone II is reached as the

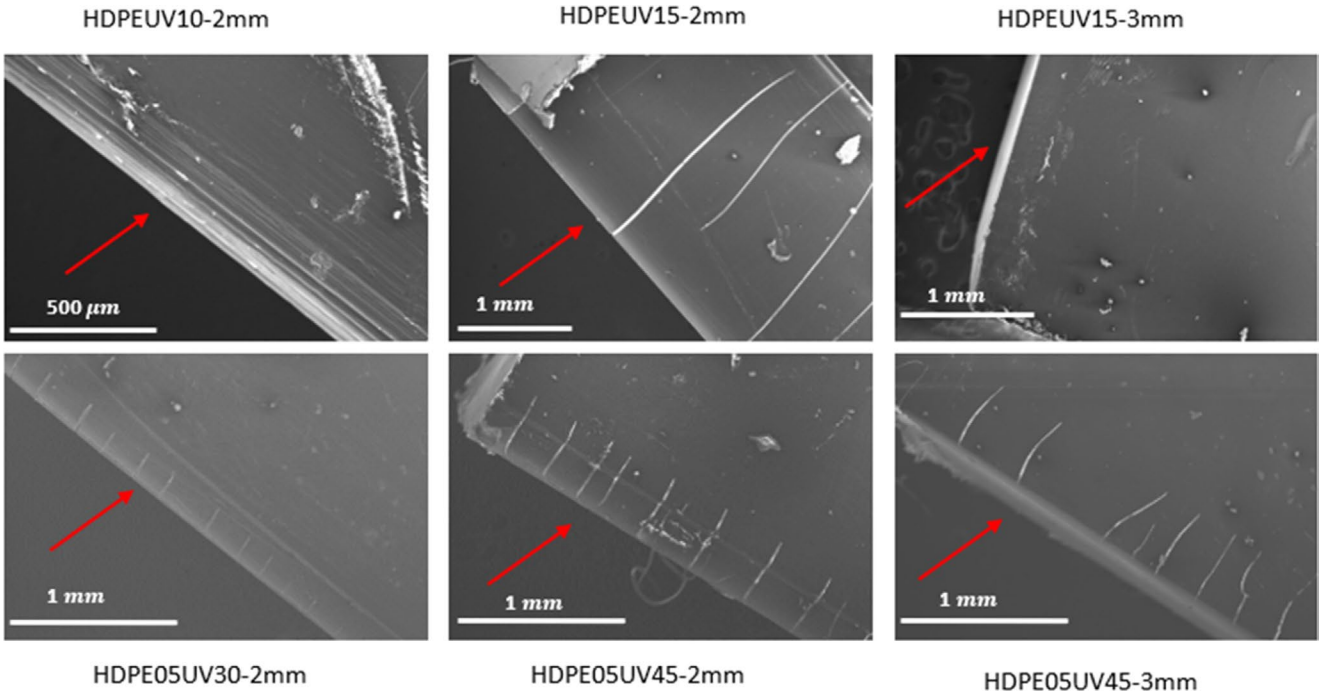

FIGURE 4 | SEM images of the side surfaces of neat HDPE and HDPE05 with sample thicknesses of 2 and 3 mm. [Color figure can be viewed at wileyonlinelibrary.com]

TABLE 3 | The observed crack depth in HDPE and HDPE05.

Sample	Crack depth (μm)
HDPEUV10-2 mm	—
HDPEUV15-2 mm	Entire thickness (2000)
HDPEUV15-3 mm	—
HDPE05UV30-2 mm	150 ± 20
HDPE05UV45-2 mm	400 ± 28
HDPE05UV45-3 mm	410 ± 80

stress falls between the first and second yield points. This zone corresponds to the onset of plastic deformation and lamella orientation [35]. Zone III starts after the second yield point, corresponding to the onset of lamella fragmentation, and it continues with the development of a necking process on the sample [35, 36]. Finally, Zone IV is characterized by a gradual increase in stress and is often denoted as the strain-hardening region [37, 38].

It can be seen in Figure 5a that as UV exposure time increases, the elongation at break consistently decreases. This promotes a gradual shift in failure from Zone IV to Zone I. These observations are related to chain scission occurring during the photodegradation of HDPE [39–41]. Notably, a shift in the failure zone and a decrease in elongation at break occur at a considerably faster rate in the 2 mm thick samples. The same trend is observed in HDPE05, where 2 mm thick samples are more sensitive to photodegradation than 3 mm thick samples. This higher sensitivity of the thinner samples is explained by the greater relative photodegradation depth, as will be shown in the next section.

The stress–strain curves were used to calculate the retention of elongation at break for neat HDPE and its composites based on Equation (6).

$$\text{Retention of elongation at break} = \frac{EB_i}{EB_0} * 100 \tag{6}$$

where EB_0 and EB_i are elongation at break before and after a certain exposure time, respectively.

Figure 6 shows the retention of elongation at break as a function of UV exposure time, the corresponding effective UV dosage (D_{eff}), and sample thickness.

It can be seen that the curves exhibit a reverse sigmoidal pattern, which includes an initial plateau followed by a steep fall, and eventually reach a second plateau [41]. The first plateau indicates the initial resistance to UV degradation, while the slope of the fall is an indication of the degradation rate. The incorporation of FLG into the composites not only prolonged the first plateau, but also reduced the slope of the declining region, indicating that it slows down both the initiation and propagation stages of photodegradation.

Neat HDPE undergoes a relatively rapid decline in elongation, reaching zero retention of elongation at break after 10 days of UV exposure for both 3- and 2-mm thick samples. As expected, the thinner samples of both HDPE and HDPE05 exhibit lower stability under UV exposure, with their retained elongation curves shifting toward shorter exposure times. This can be related to the fact that the relative degradation depth is larger in thinner samples, that is, a larger portion of the sample is affected by degradation mechanisms. Nevertheless, incorporating FLG into HDPE results in an increase in the length of the initial plateau and a more

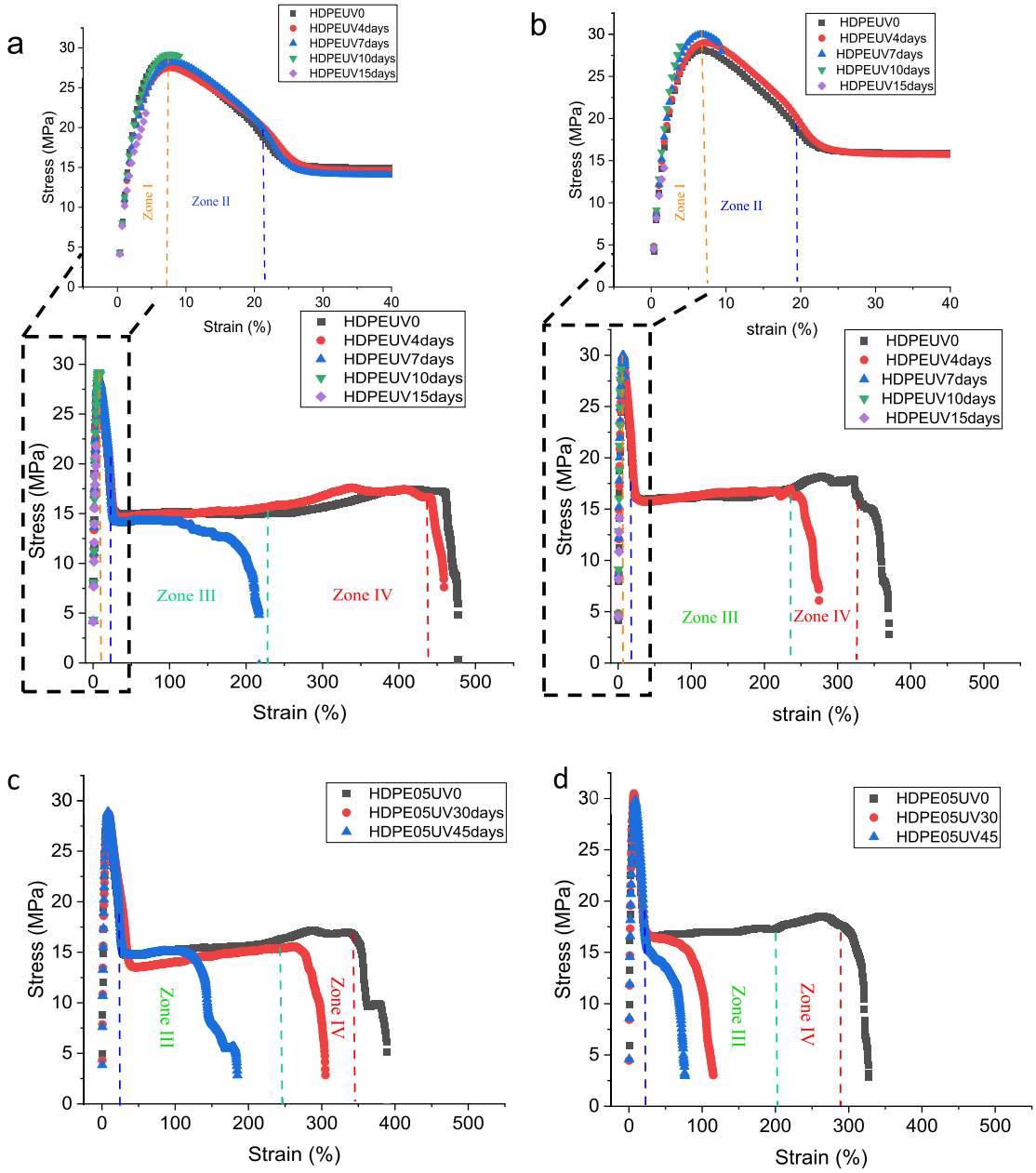

FIGURE 5 | Stress–strain curves of neat HDPE with a thickness of (a) 3 mm and (b) 2 mm, and HDPE05 with a thickness of (c) 3 mm and (d) 2 mm with different UV exposure times. [Color figure can be viewed at wileyonlinelibrary.com]

TABLE 4 | Different zones in stress–strain curves of HDPE.

Zones	Location
Zone I	Before first yield point
Zone II	Between first and second yield points
Zone III	Between second yield point and hardening points
Zone IV	Beyond hardening point

gradual decrease in retained elongation values. These comparative findings can be quantified by calculating the time it takes for a 50% reduction of the initial elongation, denoted as t_{50}. Notably, the incorporation of 0.5 wt% FLG in 3 mm thick HDPE increases t_{50} from 7 days to 45 days. Similarly, for 2 mm thick samples, t_{50} is increased from 5 days to 20 days upon the addition of 0.5 wt% FLG.

It is worth highlighting that HDPE containing FLG is slightly less ductile than neat HDPE before UV exposure. However, the composites were significantly more effective in maintaining a ductile behavior after UV exposure than neat HDPE, even at longer exposure times.

The results above indicate that the presence of FLG markedly enhances the UV stability of HDPE, even under prolonged UV exposure and regardless of sample thickness. To establish a connection between changes in mechanical properties, photodegradation depth, and microstructural changes, an in-depth investigation of crystallinity during UV exposure is presented in the next section.

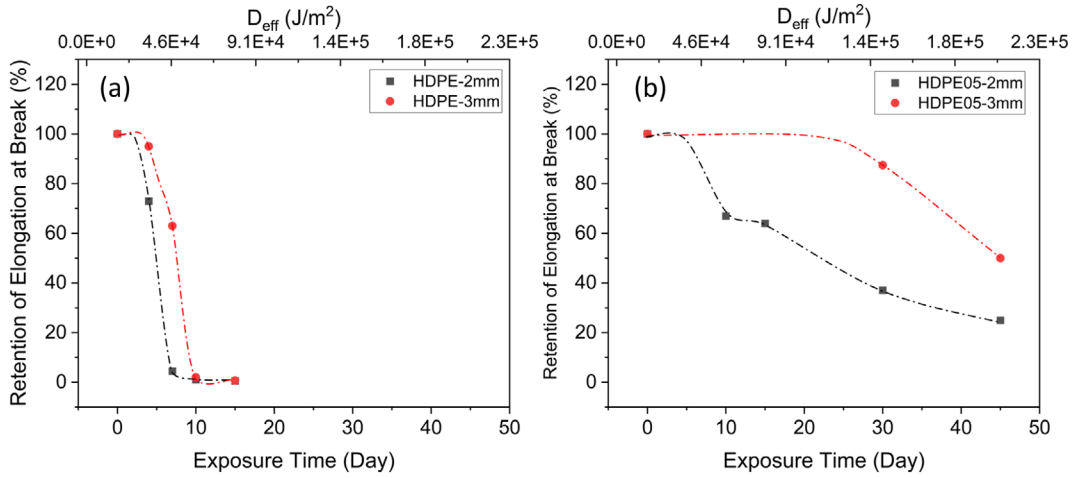

FIGURE 6 | Retention of elongation at break of (a) neat HDPE, and (b) HDPE05 with thicknesses of 3 and *2* mm as a function of exposure time and corresponding effective UV dosage. [Color figure can be viewed at wileyonlinelibrary.com]

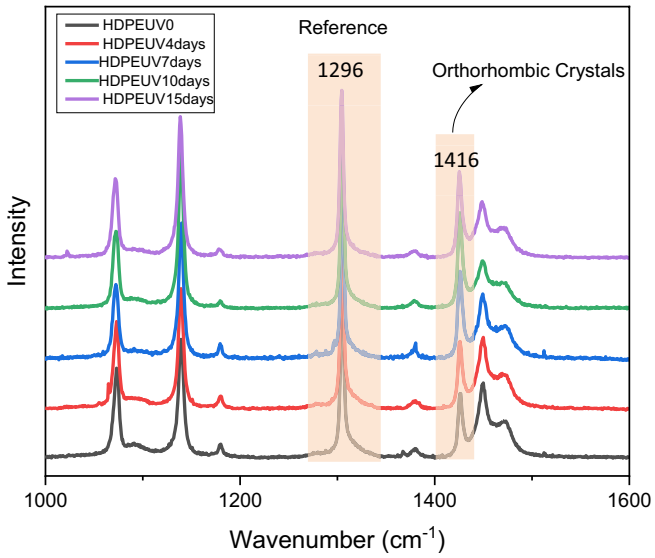

FIGURE 7 | Raman spectrum of neat HDPE exposed surface with different UV exposure times. [Color figure can be viewed at wileyonlinelibrary.com]

3.4 | Photodegradation Depth

Figure 7 shows a typical Raman spectrum of the UV-exposed surface of neat HDPE for different exposure times. The 1128 and 1062 cm^{-1} bands are assigned to the in-phase and out-of-phase stretching of C–C vibrations. The band at 1296 cm^{-1} is a C–H twisting mode associated with the all-trans –$(CH_2)_n$– chain. The region comprising 1416, 1439, and 1462 cm^{-1} bands is related to CH_2 bending vibrations. The bands at 1462, 1294, 1128, and 1062 cm^{-1} are related to the overall microstructural organization of the polymer chains, and the 1416 and 1439 cm^{-1} bands are more specifically associated with the orthorhombic crystal structure of HDPE. Thus, the band at 1416 cm^{-1} characterizes itself as a suitable marker for monitoring the chemi-crystallization process during UV exposure. The Raman bands were all normalized by the reference band located at 1296 cm^{-1}. This band was selected as a reference because it is related to the CH_2 twisting vibration in the polymer backbone, exhibiting a strong intensity and increasing the reliability of the normalization [31, 32]. It is noticeable that the 1416 cm^{-1} band increases in intensity as a function of exposure time in neat HDPE. This suggests that chemi-crystallization is taking place during UV degradation, and the formation of orthorhombic crystals is favored in the affected regions [42].

Figure 8 schematically shows the evolution of chemi-crystallization across the sample depth at different exposure times. In the context of chemi-crystallization during photodegradation, the amorphous regions of the polymer undergo a process of reorganization and ordering into crystalline structures [43]. Since chemi-crystallization occurs as a result of chain scission during UV exposure, it is a reliable indicator of photodegradation depth. To evaluate this, Raman spectroscopy coupled to an optical microscope was performed on the cross-sections of the samples, measuring the intensity of the orthorhombic crystal band at different depths. The depth where crystallinity changes due to chemi-crystallization was identified as the photodegradation depth.

Figure 9 shows a typical crystal band intensity profile, as well as the degree of crystallinity along the depth of 3- and 2-mm thick samples for different UV exposure times. More detailed data can be found in Figure S2. Figure 9 shows that the intensity of the crystal band, and consequently, the degree of crystallinity, is quite similar for both the neat material and the nanocomposite before UV exposure, independently of depth. Lower values around 38% are observed close to the surface due to the skin effect, in which cooling rate and crystal morphology are different from the bulk [44]. On the other hand, the core reaches values in the range of 60%–65% crystallinity. As the addition of 0.5 wt% FLG did not change the overall crystallinity of the material before UV exposure, any increase in crystallinity after UV exposure can be attributed to chemi-crystallization effects.

After 4 days of UV exposure, neat HDPE shows a slight increase in the crystal band intensity within the first 100–150 μm

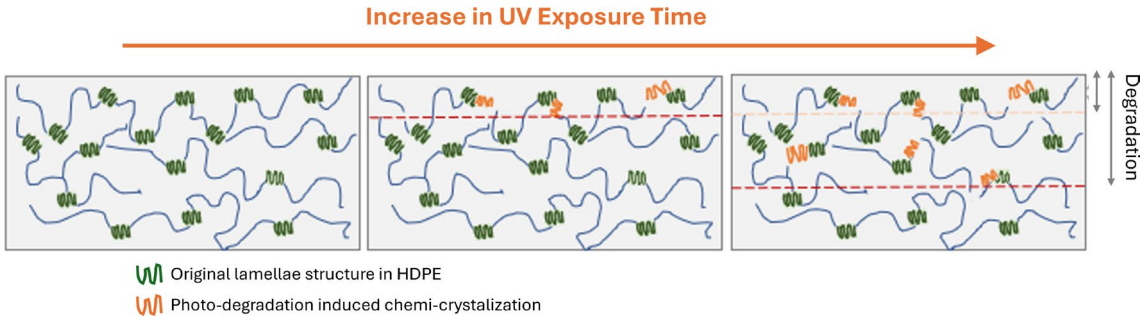

FIGURE 8 | Schematic of chemi-crystallization evolution with UV exposure time. [Color figure can be viewed at wileyonlinelibrary.com]

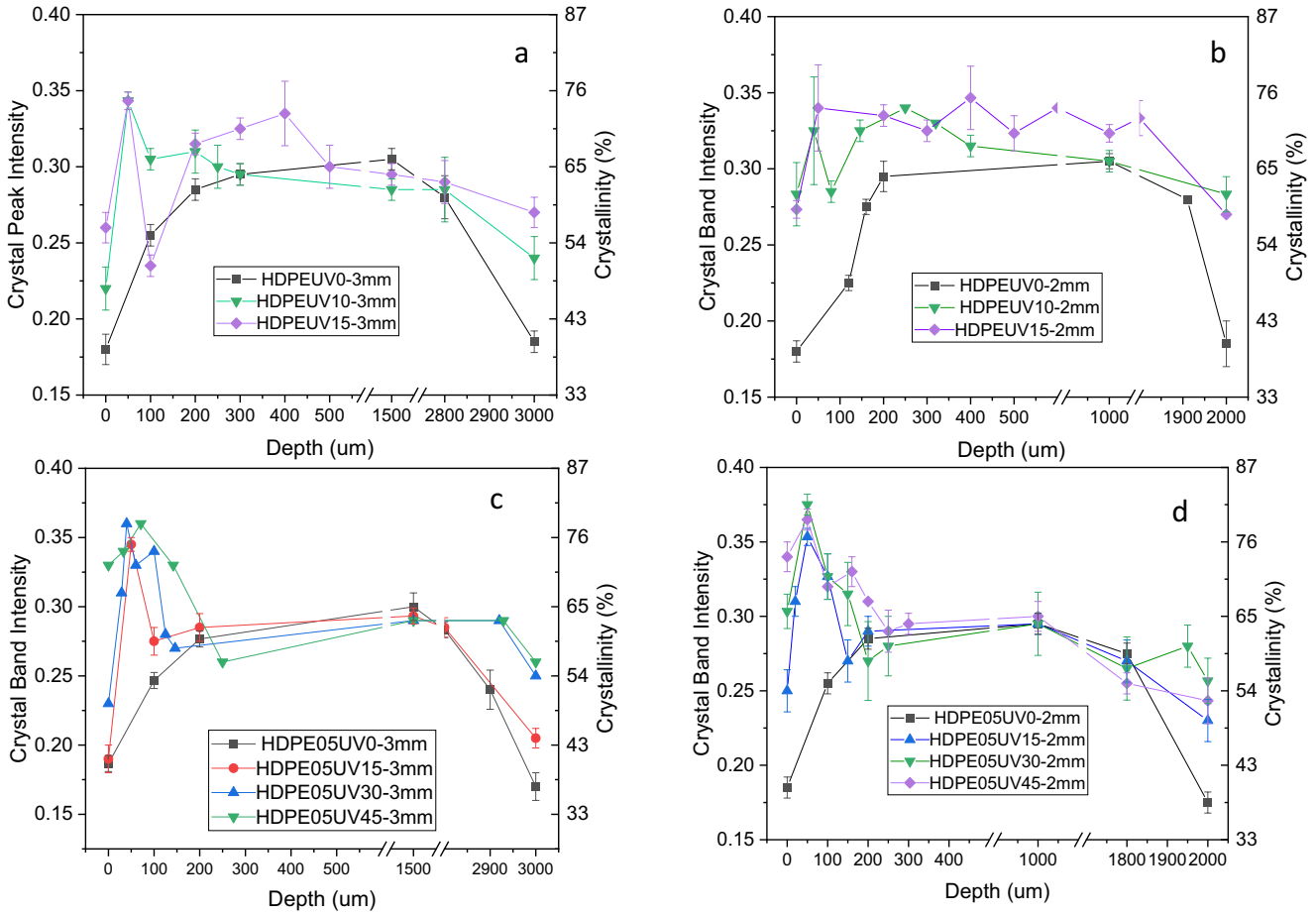

FIGURE 9 | Crystal band intensity and crystallinity profile as a function of sample depth for different UV exposure times for (a) 3 mm pure HDPE samples, (b) 2 mm pure HDPE samples, (c) 3 mm HDPE samples containing 0.5 wt% graphene, (d) 2 mm HDPE samples containing 0.5 wt% graphene. [Color figure can be viewed at wileyonlinelibrary.com]

in both 3- and 2-mm thick samples. This indicates chemi-crystallization occurred in this region. However, the samples remain unaffected at greater depths. It is worth emphasizing that the slightly higher crystallinity observed on the back-face of the samples is due to the faster development of photodegradation processes at the surface than in the bulk, which can lead to chemi-crystallization on the back-face of the samples. After 10 days of UV exposure, the affected depth increases to 300 and 400 μm in neat HDPE-3 mm and neat HDPE-2 mm, respectively. Subsequently, after 15 days of UV exposure, the affected depth is extended to 500 μm in neat HDPE-3 mm, while an increase in the crystal band intensity is observed throughout the entire sample depth in neat HDPE-2 mm.

As can be seen in Figure S2, the increase in the crystal band intensity and affected depth for HDPE05 becomes apparent only after 15 and 10 days of UV exposure for the 3- and 2-mm thick samples, respectively. This reveals the remarkable stabilizing effect of FLG in preventing photodegradation-induced microstructural changes.

The photodegradation depth (D) is identifiable in Figure 9, where the polymer's degraded layer undergoes chemi-crystallization, resulting in increased crystallinity relative to the unexposed material at each corresponding depth. It is important to note that the failure of a sample is intrinsically linked to the ratio of photodegradation depth (D) and

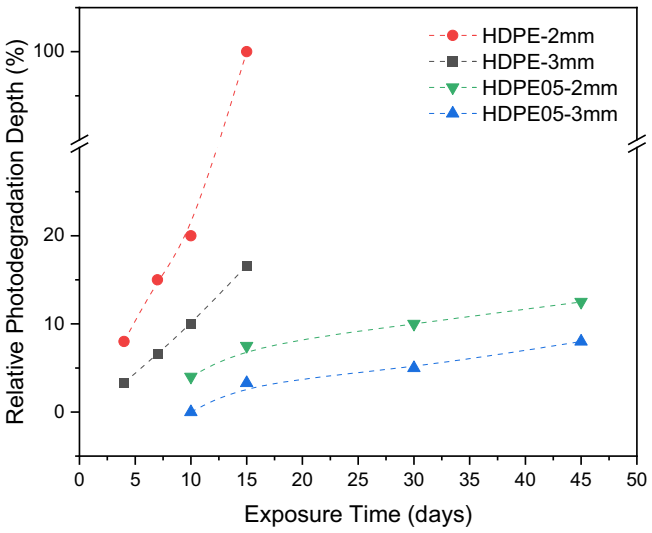

FIGURE 10 | Relative photodegradation depth as a function of exposure time for neat HDPE and HDPE05 composites. [Color figure can be viewed at wileyonlinelibrary.com]

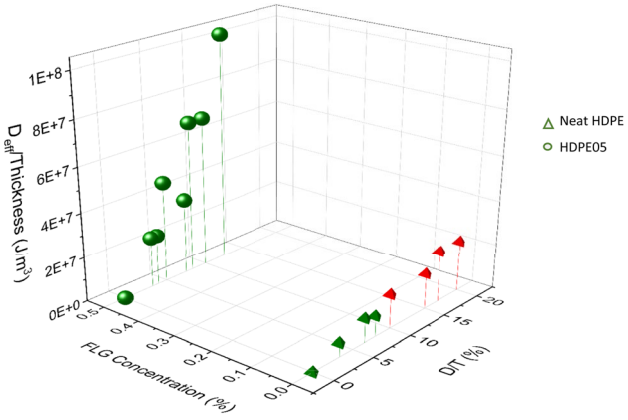

FIGURE 11 | Failure behavior of neat HDPE and HDPE05 as a function of UV dosage and relative photodegradation depth. The green color represents ductile behavior (Zone III and IV), and the red color indicates the brittle behavior (Zone I and II). [Color figure can be viewed at wileyonlinelibrary.com]

its thickness (T), that is, the relative photodegradation depth, which is calculated according to Equation (7) and is presented in Figure 10.

$$\text{Relative photodegradation depth}\,(\%) = {}^{D}/_{T} \times 100 \quad (7)$$

When the relative photodegradation depth is analyzed, the effect of adding FLG on the stability of HDPE under UV exposure becomes evident. While the 3-mm thick HDPE sample reached a D/T of 16.7% after 15 days of exposure, the 2-mm thick HDPE sample exhibited a D/T of 100% after just 10 days of exposure. On the other hand, the 3- and 2-mm HDPE05 samples reached D/T values of only 6.7% and 12.5%, respectively, after 45 days of exposure. Following the determination of D/T, this parameter was effectively employed to analyze the samples' embrittlement. This analysis and its findings are detailed in the following section.

3.5 | Failure Behavior Based on Relative Degradation Depth (D/T)

The experimental failure behavior of neat HDPE and HDPE05, based on the relative photodegradation depth and UV dosage per sample volume, is presented in Figure 11. The samples that exhibited ductile behavior (fracture in Zone III or IV) are shown in green. The samples that exhibited brittle behavior (fracture in Zone I or II) are in red. As expected, the higher the relative photodegradation depth in HDPE, the more brittle the material's behavior due to the deeper changes in the microstructure.

Embrittlement happens at D/T values of around 10% in neat HDPE, which takes place at a dosage of $1.6\times10^{7}\,J/m^{3}$. On the other hand, HDPE05 sustained a ductile failure even at much higher UV dosages ($1\times10^{8}\,J/m^{3}$), that is, more than five times higher than that of neat HDPE, while also maintaining a low relative photodegradation depth of just 12.5%. These results highlight the FLG photo-stabilizing effect on HDPE, preventing brittle failure in the composites even at higher UV dosage.

4 | Discussion

In this study, a notable enhancement in the UV stability of HDPE composites was achieved through the incorporation of FLG. Retention of elongation at break was calculated for neat HDPE and its composites as a function of sample thickness, exposure time, and corresponding UV dosage. The retention curves exhibited a reverse sigmoidal shape, with significant changes in the presence of FLG. Not only was the first plateau extended, indicating a delay in the initiation step, but the slope of the curve decreased significantly, demonstrating a deceleration in the propagation step. These results are in good alignment with our previous work, which confirmed that FLG can act as both UV absorber/reflector and free radical scavenger, effectively preventing both the initiation and propagation steps [8]. Moreover, the HDPE05 retention of elongation at break curves displays a tendency to reach a nonzero plateau, even at higher exposure times. This suggests a unique and promising potential of HDPE05 to maintain ductile behavior even after significant exposure to UV radiation, as the degraded layer remains restricted to the surface due to a lower initial crystallinity and a scarcity of FLG in that region. This hypothesis is corroborated by the Raman analysis, where it was identified that the degraded layer did not exceed 12.5% and 6.7% of the sample thickness for 2- and 3-mm thick HDPE05, respectively, even after 45 days of weathering.

A correlation between microstructural changes and embrittlement was established in neat HDPE and its composites containing 0.5 wt% FLG. In neat HDPE-3 mm, chemi-crystallization occurred primarily within the first 500 μm of the sample thickness after 15 days of UV exposure, indicating an upper limit for photodegradation depth within this range. This result is in good agreement with previous studies on LDPE [45] and HDPE [46], in which the amount of degradation species showed a sharp decrease with the sample thickness, suggesting an oxygen diffusion-controlled condition during photodegradation [38]. HDPE-2 mm presented an oxygen diffusion-controlled degradation behavior only up to 10 days of UV exposure. After 15 days of UV exposure, chemi-crystallization extended throughout

the entire thickness of the sample, potentially facilitated by the cracks created, which exposed more surface to UV radiation [47] and facilitated oxygen to diffuse deeper into the sample. In the case of HDPE05, chemi-crystallization took place only within the first 250 μm independently of sample thickness, even after 45 days of UV exposure. The more limited photodegradation in HDPE05 compared to that of neat HDPE is attributed to the photo-stabilizing effect of FLG.

The photodegradation depth was normalized by the sample thickness and correlated with the materials' embrittlement as a function of UV dosage per sample volume, as is illustrated in Figure 10. Notably, the embrittlement occurred in neat HDPE when the relative photodegradation depth reached ~10%, even before the appearance of visible cracks, as was observed by SEM. This embrittlement was observed at a remarkably low value of UV dosage, that is, below 2×10^7 J/m^3, which is equivalent to 7–10 days of UV exposure. In fact, HDPE, characterized by plastic deformation under tension [38, 48–50], typically initiates plastic deformation after surpassing the second yield point. At the second yield point, tie molecules transfer the load to the crystal structures and initiate plastic deformation through lamella slipping and fragmentation [51, 52]. Embrittlement occurs when the material fails to progress beyond the second yield point and effectively transfer the load to the crystal structures. Photodegradation induces chemi-crystallization and chain scission, consequently disrupting the tie molecules from transferring the load to crystal structures. In turn, this results in a reduction of elongation at break and, therefore, embrittlement. By correlating the tensile behavior with the degree of crystallinity estimated from Raman analysis, this study revealed that embrittlement occurs when chemi-crystallization induced by photodegradation reaches ~10% of the sample thickness in neat HDPE. However, the incorporation of 0.5 wt% FLG led to a remarkable resistance to embrittlement. Interestingly, despite the formation of surface cracks at extended exposure times, as was observed in SEM images, HDPE05 maintained its ductile behavior on the tensile tests. Therefore, the photo-stabilizing effect of FLG may not be the only contributor to the sustained ductile behavior. To more adequately describe this behavior, it is necessary to consider the formation of surface cracks in the presence of FLG.

The formation of cracks during photodegradation is known to originate from shrinkage and mechanical stress caused by chain scission and crosslinking [53]. When FLG is present, it increases sample heterogeneity, density, and mechanical stress [54], which could lead to the appearance of surface cracks under UV exposure. In the composite samples, photodegradation initiates near the surface, which is deprived of FLG, as was shown in Figure 2. As cracks form at a higher density in regions with low FLG concentration, as shown in Figure 4, when these cracks begin to propagate deeper into the sample, they are effectively arrested by the FLG-rich regions. This limits their progression, confining them near the surface and preventing further penetration into the material. Consequently, the embrittled layer becomes isolated from the ductile core, allowing the composite to maintain ductile behavior even when the relative degradation depth is larger. This is evident in the retained elongation curve of HDPE05-2 mm, where a nonzero plateau indicates sustained ductility despite the microstructural effects of photodegradation. This behavior was previously observed in the photodegradation of polypropylene (PP)/talc systems, contributing to the detachment of the degraded layer [34, 55, 56]. These features are especially valuable for outdoor applications, as the UV resistance conferred by FLG can substantially extend the component's service life under continuous environmental exposure. Nevertheless, future studies should broaden the experimental scope by exploring a wider range of FLG contents and sample thicknesses, thereby enabling the determination of the optimal FLG concentration relative to part thickness.

5 | Conclusion

In this study, the effect of adding FLG on the photodegradation depth of HDPE was investigated. Photodegradation depth and chemi-crystallization that occurs across the sample were correlated to the transition from ductile to brittle tensile behavior. The results showed that embrittlement occurred in neat HDPE when the relative photodegradation depth reached only 10% of the sample thickness for both 3- and 2-mm thick samples. Notably, this embrittlement was observed in neat HDPE even before the formation of surface cracks. In contrast, HDPE containing 0.5 wt% FLG showed ductile behavior even at significantly higher UV dosages, that is, up to 45 days of UV exposure. Interestingly, the ductile behavior was maintained even when the relative photodegradation depth exceeded the 10% threshold and surface cracks were present. This behavior is attributed to the photo-stabilizing effect of FLG through its multifunctionality acting on different fronts, that is, UV shielding, barrier effect, and radical scavenging, as well as the isolation of the embrittled surface layer from the sample's ductile core. In summary, incorporation of 0.5 wt% FLG into the polymer matrix extended the embrittlement threshold for relative degradation depth from 10% to over 12.5%, as well as the UV dosage needed to reach such threshold from 1.6×10^7 to over 1×10^8 J/m^3. This allows the material to endure extended UV exposure without succumbing to embrittlement, which has great significance for HDPE materials used in outdoor packaging and coating applications.

Author Contributions

Samira Karimi: conceptualization (equal), data curation (lead), formal analysis (lead), investigation (lead), methodology (lead), writing – original draft (lead). **Emna Helal:** conceptualization (equal), project administration (equal), supervision (supporting), writing – review and editing (equal). **Gabriel Matheus Pinto:** investigation (equal), validation (equal), visualization (equal), writing – review and editing (lead). **Giovanna Gutierrez:** conceptualization (equal), funding acquisition (equal), project administration (equal), resources (equal), supervision (supporting), writing – review and editing (supporting). **Nima Moghimian:** funding acquisition (equal), project administration (supporting), resources (equal), supervision (supporting). **Tatiana Parra Vello:** formal analysis (equal), investigation (equal), methodology (equal), writing – review and editing (supporting). **Guilhermino José Macêdo Fechine:** project administration (equal), supervision (equal), writing – review and editing (equal). **Eric David:** funding acquisition (supporting), project administration (supporting), resources (supporting), supervision (equal), writing – review and editing (equal). **Nicole Demarquette:** conceptualization (equal), funding acquisition (lead), project administration (lead), resources (lead), writing – review and editing (equal).

Acknowledgments

The authors would like to acknowledge the financial support of the Natural Sciences and Engineering Research Council of Canada (NSERC) (Grant CRDPJ 538482-18), the NanoXplore Inc., and the Canadian Research Chair CRC Tier 1-2021-00489. During the preparation of this work, the authors used ChatGPT to improve the readability and language of the manuscript. After using this tool/service, the authors reviewed and edited the content as needed and took full responsibility for the content of the publication.

Conflicts of Interest

The authors declare no conflicts of interest.

Data Availability Statement

The data that support the findings of this study are available from the corresponding author upon reasonable request.

References

1. N. Allen and J. McKellar, "Photodegradation and Stabilization of Commercial Polyolefins," *Chemical Society Reviews* 4, no. 4 (1975): 533–547.

2. J. White and A. Turnbull, "Weathering of Polymers: Mechanisms of Degradation and Stabilization, Testing Strategies and Modelling," *Journal of Materials Science* 29 (1994): 584–613.

3. R. Raad and M. Abdallh, "Surface Modification to Enhance Photo-Stability of Polymers," *GSC Advanced Research and Reviews* 11, no. 2 (2022): 80–88.

4. Y. H. So, "Photodegradation Mechanism and Stabilization of Polyphenylene Oxide and Rigid-Rod Polymers," *Polymer International* 55, no. 2 (2006): 127–138.

5. S. Karimi, E. Helal, G. Gutierrez, et al., "A Review on Graphene's Light Stabilizing Effects for Reduced Photodegradation of Polymers," *Crystals* 11, no. 1 (2020): 3.

6. Y. D. de Oliveira, L. G. Amurin, F. C. Valim, G. J. Fechine, and R. J. Andrade, "The Role of Physical Structure and Morphology on the Photodegradation Behaviour of Polypropylene-Graphene Oxide Nanocomposites," *Polymer* 176 (2019): 146–158.

7. M. I. Tayouri, S. Estaji, S. R. Mousavi, et al., "Degradation of Polymer Nanocomposites Filled With Graphene Oxide and Reduced Graphene Oxide Nanoparticles: A Review of Current Status," *Polymer Degradation and Stability* 206 (2022): 110179.

8. S. Karimi, E. Helal, G. Gutierrez, et al., "Photo-Stabilization Mechanisms of High-Density Polyethylene (HDPE) by a Commercial Few-Layer Graphene," *Polymer Engineering & Science* 63, no. 11 (2023): 3879–3890.

9. M. Mistretta, L. Botta, A. Vinci, M. Ceraulo, and F. La Mantia, "Photo-Oxidation of Polypropylene/Graphene Nanoplatelets Composites," *Polymer Degradation and Stability* 160 (2019): 35–43.

10. S. Amrollahi, B. Ramezanzadeh, H. Yari, M. Ramezanzadeh, and M. Mahdavian, "In-Situ Growth of Ceria Nanoparticles on Graphene Oxide Nanoplatelets to Be Used as a Multifunctional (UV Shield/Radical Scavenger/Anticorrosive) Hybrid Compound for Exterior Coatings," *Progress in Organic Coatings* 136 (2019): 105241.

11. S. Uran, A. Alhani, and C. Silva, "Study of Ultraviolet-Visible Light Absorbance of Exfoliated Graphite Forms," *AIP Advances* 7, no. 3 (2017): 035323.

12. D. G. Goodwin, Jr., S. J. Shen, Y. Lyu, et al., "Graphene/Polymer Nanocomposite Degradation by Ultraviolet Light: The Effects of Graphene Nanofillers and Their Potential for Release," *Polymer Degradation and Stability* 182 (2020): 109365.

13. S. N. Sultana, E. Helal, G. Gutiérrez, E. David, N. Moghimian, and N. R. Demarquette, "The Influence of a Commercial Few-Layer Graphene on the Photodegradation Resistance of a Waste Polyolefins Stream and Prime Polyolefin Blends," *Recycling* 9, no. 2 (2024): 29.

14. Y. He, D. Fan, J. Chen, et al., "Multiple Stabilization Roles of Thermally Reduced Graphene Oxide for Both Thermo- and Photo-Oxidation of Polypropylene: Deter, Delay, and Defend," *Polymers for Advanced Technologies* 33, no. 2 (2022): 505–513.

15. A. Shyichuk, J. White, I. Craig, and I. Syrotynska, "Comparison of UV-Degradation Depth-Profiles in Polyethylene, Polypropylene and an Ethylene–Propylene Copolymer," *Polymer Degradation and Stability* 88, no. 3 (2005): 415–419.

16. M. Rabello and J. White, "Crystallization and Melting Behaviour of Photodegraded Polypropylene—I. Chemi-Crystallization," *Polymer* 38, no. 26 (1997): 6379–6387.

17. B. Fayolle, X. Colin, L. Audouin, and J. Verdu, "Mechanism of Degradation Induced Embrittlement in Polyethylene," *Polymer Degradation and Stability* 92, no. 2 (2007): 231–238.

18. Q. Deshoulles, M. le Gall, C. Dreanno, et al., "Origin of Embrittlement in Polyamide 6 Induced by Chemical Degradations: Mechanisms and Governing Factors," *Polymer Degradation and Stability* 191 (2021): 109657.

19. E. Gauthier, B. Laycock, F.-M. Cuoq, P. Halley, and K. George, "Correlation Between Chain Microstructural Changes and Embrittlement of LLDPE-Based Films During Photo- and Thermo-Oxidative Degradation," *Polymer Degradation and Stability* 98, no. 1 (2013): 425–435.

20. A. F. Reano, A. Guinault, E. Richaud, and B. Fayolle, "Polyethylene Loss of Ductility During Oxidation: Effect of Initial Molar Mass Distribution," *Polymer Degradation and Stability* 149 (2018): 78–84.

21. A. K. Rodriguez, B. Mansoor, G. Ayoub, X. Colin, and A. A. Benzerga, "Effect of UV-Aging on the Mechanical and Fracture Behavior of Low Density Polyethylene," *Polymer Degradation and Stability* 180 (2020): 109185.

22. T. Turton and J. White, "Effect of Stabilizer and Pigment on Photo-Degradation Depth Profiles in Polypropylene," *Polymer Degradation and Stability* 74, no. 3 (2001): 559–568.

23. I. Craig and J. White, "Crystallization and Chemi-Crystallization of Recycled Photodegraded Polyethylenes," *Polymer Engineering and Science* 45, no. 4 (2005): 588–595.

24. J. Gulmine, P. Janissek, H. Heise, and L. Akcelrud, "Degradation Profile of Polyethylene After Artificial Accelerated Weathering," *Polymer Degradation and Stability* 79, no. 3 (2003): 385–397.

25. T. Lu, E. Solis-Ramos, Y. Yi, and M. Kumosa, "UV Degradation Model for Polymers and Polymer Matrix Composites," *Polymer Degradation and Stability* 154 (2018): 203–210.

26. J. W. Martin, T. Nguyen, E. Byrd, B. Dickens, and N. Embree, "Relating Laboratory and Outdoor Exposures of Acrylic Melamine Coatings: I. Cumulative Damage Model and Laboratory Exposure Apparatus," *Polymer Degradation and Stability* 75, no. 1 (2002): 193–210.

27. J. W. Martin, "Quantitative Characterization of Spectral Ultraviolet Radiation-Induced Photodegradation in Coating Systems Exposed in the Laboratory and the Field," *Progress in Organic Coatings* 23, no. 1 (1993): 49–70.

28. S. W. Bigger and O. Delatycki, "The Effect of Hindered Amine Light Stabilizers on the Photooxidative Stability of High-Density Polyethylene," *Journal of Polymer Science Part A: Polymer Chemistry* 27, no. 1 (1989): 63–73.

29. S. W. Bigger and O. Delatycki, "The Effects of Pigments on the Photostability of Polyethylene," *Journal of Materials Science* 24 (1989): 1946–1952.

30. B. C. Daglen and D. R. Tyler, "Photodegradable Plastics: End-of-Life Design Principles," *Green Chemistry Letters and Reviews* 3, no. 2 (2010): 69–82.

31. C. C. Naylor, R. J. Meier, B. J. Kip, et al., "Raman Spectroscopy Employed for the Determination of the Intermediate Phase in Polyethylene," *Macromolecules* 28, no. 8 (1995): 2969–2978.

32. G. R. Strobl and W. Hagedorn, "Raman Spectroscopic Method for Determining the Crystallinity of Polyethylene," *Journal of Polymer Science, Polymer Physics Edition* 16, no. 7 (1978): 1181–1193.

33. W. Lin, M. Cossar, V. Dang, and J. Teh, "The Application of Raman Spectroscopy to Three-Phase Characterization of Polyethylene Crystallinity," *Polymer Testing* 26, no. 6 (2007): 814–821.

34. M. Rabello and J. White, "The Role of Physical Structure and Morphology in the Photodegradation Behaviour of Polypropylene," *Polymer Degradation and Stability* 56, no. 1 (1997): 55–73.

35. N. Brooks, A. Unwin, R. Duckett, and I. Ward, "Double Yield Points in Polyethylene: Structural Changes Under Tensile Deformation," *Journal of Macromolecular Science, Part B: Physics* 34, no. 1–2 (1995): 29–54.

36. R. Séguéla, "On the Natural Draw Ratio of Semi-Crystalline Polymers: Review of the Mechanical, Physical and Molecular Aspects," *Macromolecular Materials and Engineering* 292, no. 3 (2007): 235–244.

37. K.-H. Nitta and M. Kuriyagawa, "Application of Catastrophe Theory to Neck Initiation of Metallocene-Catalyzed High-Density Polyethylene," *Polymer Journal* 44, no. 3 (2012): 245–251.

38. A. Peterlin, "Molecular Model of Drawing Polyethylene and Polypropylene," *Journal of Materials Science* 6 (1971): 490–508.

39. I. Grigoriadou, K. Paraskevopoulos, K. Chrissafis, E. Pavlidou, T.-G. Stamkopoulos, and D. Bikiaris, "Effect of Different Nanoparticles on HDPE UV Stability," *Polymer Degradation and Stability* 96, no. 1 (2011): 151–163.

40. H.-C. Hsueh, J. H. Kim, S. Orski, et al., "Micro and Macroscopic Mechanical Behaviors of High-Density Polyethylene Under UV Irradiation and Temperature," *Polymer Degradation and Stability* 174 (2020): 109098.

41. A. Fairbrother, H. C. Hsueh, J. H. Kim, et al., "Temperature and Light Intensity Effects on Photodegradation of High-Density Polyethylene," *Polymer Degradation and Stability* 165 (2019): 153–160.

42. Y. Hiejima, T. Kida, K. Takeda, T. Igarashi, and K.-h. Nitta, "Microscopic Structural Changes During Photodegradation of Low-Density Polyethylene Detected by Raman Spectroscopy," *Polymer Degradation and Stability* 150 (2018): 67–72.

43. I. Craig, J. White, and P. C. Kin, "Crystallization and Chemi-Crystallization of Recycled Photo-Degraded Polypropylene," *Polymer* 46, no. 2 (2005): 505–512.

44. M. R. Kamal and F. H. Moy, "Microstructural Characterization of Injection-Molded Articles," *Journal of Applied Polymer Science* 28, no. 5 (1983): 1787–1804.

45. A. L. Andrady, K. L. Law, J. Donohue, and B. Koongolla, "Accelerated Degradation of Low-Density Polyethylene in Air and in Sea Water," *Science of the Total Environment* 811 (2022): 151368.

46. V. Moreno-Serna, M. Ubilla, L. Montoille, et al., "Influence of Modified SiO_2 Nanoparticles on the Photostability of Recycled HDPE," *Journal of Polymers and the Environment* 32 (2023): 1–14.

47. I. Yakimets, D. Lai, and M. Guigon, "Effect of Photo-Oxidation Cracks on Behaviour of Thick Polypropylene Samples," *Polymer Degradation and Stability* 86, no. 1 (2004): 59–67.

48. L. Lin and A. Argon, "Structure and Plastic Deformation of Polyethylene," *Journal of Materials Science* 29 (1994): 294–323.

49. N. Brusselle-Dupend and L. Cangémi, "A Two-Phase Model for the Mechanical Behaviour of Semicrystalline Polymers. Part I: Large Strains Multiaxial Validation on HDPE," *Mechanics of Materials* 40, no. 9 (2008): 743–760.

50. A. Pawlak, "Cavitation During Tensile Deformation of High-Density Polyethylene," *Polymer* 48, no. 5 (2007): 1397–1409.

51. Y.-C. Hsu, M. P. Weir, R. W. Truss, C. J. Garvey, T. M. Nicholson, and P. J. Halley, "A Fundamental Study on Photo-Oxidative Degradation of Linear Low Density Polyethylene Films at Embrittlement," *Polymer* 53, no. 12 (2012): 2385–2393.

52. A. Rozanski and A. Galeski, "Plastic Yielding of Semicrystalline Polymers Affected by Amorphous Phase," *International Journal of Plasticity* 41 (2013): 14–29.

53. F. Awaja, S. Zhang, M. Tripathi, A. Nikiforov, and N. Pugno, "Cracks, Microcracks and Fracture in Polymer Structures: Formation, Detection, Autonomic Repair," *Progress in Materials Science* 83 (2016): 536–573.

54. Z. Al-Maqdasi, L. Pupure, G. Gong, N. Emami, and R. Joffe, "Time-Dependent Properties of Graphene Nanoplatelets Reinforced High-Density Polyethylene," *Journal of Applied Polymer Science* 138, no. 30 (2021): 50783.

55. M. Rabello and J. White, "Photodegradation of Talc-Filled Polypropylene," *Polymer Composites* 17, no. 5 (1996): 691–704.

56. M. Rabello and J. White, "Photodegradation of Polypropylene Containing a Nucleating Agent," *Journal of Applied Polymer Science* 64, no. 13 (1997): 2505–2517.

Supporting Information

Additional supporting information can be found online in the Supporting Information section. **Table S1:** app70044-sup-0001-supinfo.docx. **Table S2:** app70044-sup-0001-supinfo.docx. **Figure S1:** app70044-sup-0001-supinfo.docx. **Figure S2:** app70044-sup-0001-supinfo.docx.